Holographic Waveguide Display With Large Field of View and High Light Efficiency Based on Polarized Volume Holographic Grating

Yuchen Gu, Yishi Weng, Ran Wei, Zhongwen Shen ⓘ, Chuang Wang, LiXuan Zhang, and Yuning Zhang ⓘ

Abstract—We propose a polarization multiplexing structure based on multilayer reflective polarized volume holographic gratings(PVGs) to improve the field of view and brightness of the augmented reality waveguide display. The multilayer structure forms the splicing of different response bandwidths by stacking PVGs with different periodic components, and realizes the expansion of the wavelength (angle) bandwidth. The polarization multiplexing structure controls the polarization of the diffracted light by controlling the rotation direction of the liquid crystal pitch in the liquid crystal material, so that both left-hand and right-hand circularly polarized light are diffracted to enhance efficiency. Based on these two structures, the wavelength bandwidth of PVG is increased by 40 nm, the angular bandwidth is increased by 10° and the diffraction efficiency is nearly doubled. In order to verify the feasibility of these two structures, we use the holographic waveguide display with OLED as the image source. The demonstrated waveguide prototype shows a complete display with a diagonal field of view of 55°. The brightness of virtual image was measured as high as 1100 cd/m² with a transparency of 72% for ambient light.

Index Terms—Augmented reality, polarized volume holographic grating, field of view, light efficiency.

I. INTRODUCTION

WITH the development of new technologies such as 5G communications, big data, cloud computing and artificial intelligence, the application scenarios of visual displays have become more diversified, and the form of displays is also constantly innovating. Augmented reality(AR) can superimpose digital information on real scene, bringing the combination of virtual world and real world [1]. Many scientific research institutions and companies have been attracted, and they have launched research on AR-related technology [2]. As the most critical and scarce core component of the AR display system, the optical combiner influences the field of view (FOV), optical efficiency, exit pupil size and other parameters, which affect the performance of the entire display system. Currently, the more mainstream technical solutions include beam splitting prism [3], free-form surface [4], Maxwellian display [5], [6] and optical waveguide [7]. The optical waveguide can obtain a larger eye movement range while keeping its volume and weight as small as possible, which is considered to be the most promising technical solution.

The optical coupling element is the most critical optical element in the optical waveguide technology. Its function is to couple the image generated by the image source into the waveguide and out of the waveguide. Partial mirror array (PRMA) [8], volume holographic grating (VHG) [9] and surface relief grating (SRG) [10] are three common solutions for optical waveguide technology. PRMA manufacturing process requirements are extremely high, resulting in a generally low product yield rate. VHG has problems with FOV and color display due to their small bandwidth, and SRG has high cost due to the complex process flow and expensive processing equipment. Compared with these three, the polarized volume holographic grating (PVG) has the advantages of large wavelength/angular bandwidth and simple manufacturing process. Weng *et al.* reported a PVG and investigated its diffraction characteristics through simulation [11]. Subsequently, Weng *et al.* designed and successfully prepared a color waveguide display prototype based on reflective PVG [12], which achieved a 35° diagonal color imaging. Kun Yin *et al.* prepared PVG on flexible materials(PDMS) and realized PVG transfer technology [13]. He Z *et al.* studied the different optical properties of planar and slanted PVG [14]. Kun Yin *et al.* report a reflective chirped polarization volume(CPVG)that can achieve an angular bandwidth of 54° [15]. Cui *et al.* simulated and prepared a two-dimensional exit pupil expansion based on reflective PVG [16]. Tao Zhan *et al.* reviewed the working principles of Pancharatnam–Berry phase optical elements(PBOEs) such as PVG and discussed the application of PBOEs in emerging display systems [17].

FOV represents the angle range of the actual display screen (virtual image) to the pupil of the human eye. The monocular FOV of human eye is about 160° in the horizontal direction, and the monocular FOV in the vertical direction is about 130°. The binocular FOV can reach approximately 200° (horizontal) × 120° (vertical) [18]. At present, the main factors limiting FOV in optical waveguide technology are the angular bandwidth of

The authors are with the Joint International Research Laboratory of Information Display and Visualization, School of Electronic Science and Engineering, Southeast University, Nanjing 210096, China (e-mail: 220191359@ seu.edu.cn; wings@seu.edu.cn; rwei317@seu.edu.cn; 220151185@seu.edu.cn; 220191379@seu.edu.cn; 220201533@seu.edu.cn; zyn@seu.edu.cn).
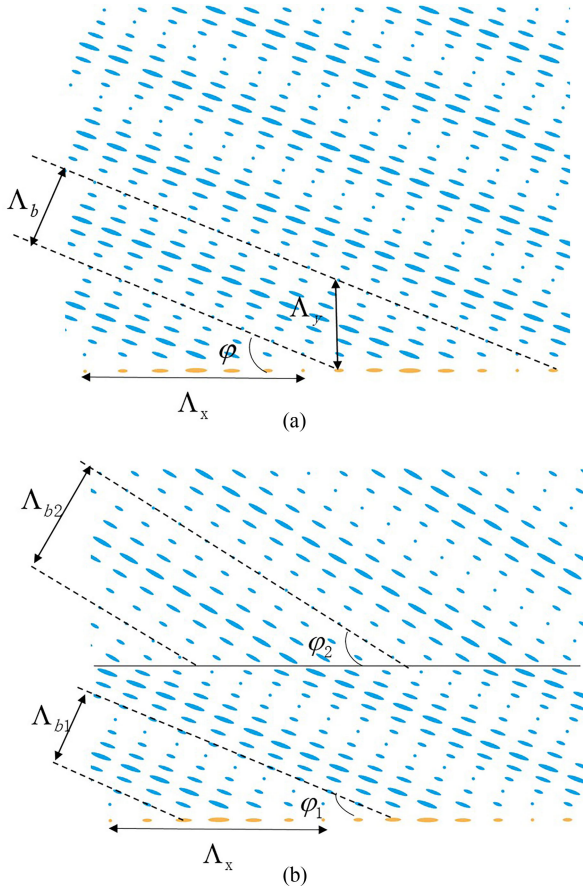
Fig. 1. LC director profile of (a) PVG. (b) LCOM-PVGs.

the grating coupler and the refractive index of the waveguide medium. Although PVG has a larger angular bandwidth than VHG, a single PVG cannot meet the requirements of a large field of view. Kun Yin *et al.* simulated and experimentally verified the feasibility of the multi-layer structure [19]. Xiao Xiang *et al.* prepared a two-layer transmissive PVG structure and tested its optical properties [20]. To the best of our knowledge, the preparation principle and process of multi-layer reflective PVG and the application of waveguide display have not been reported before.

In order to optimize FOV limited by bandwidth, this paper designs the laminated composite PVGs(LCOM-PVGs) based on reflective PVG to expand the bandwidth. At the same time, due to the polarization characteristics of PVG, PVG with a single chiral rotation as a coupler has a greater efficiency loss to AR display. To overcome this problem, a polarization multiplexing structure is designed and prepared to ensure the optical efficiency of AR holographic waveguide system. Finally, a LCOM-PVGs combined with polarization multiplexing structure was prepared, and its good performance was demonstrated on the AR display.

II. MATERIALS AND METHODS

As shown in Fig. 1(a), the structure of PVG presents a slanted structure [21], [22]. In the figure, the period in the x-direction is called the horizontal period (Λ_x), and the period
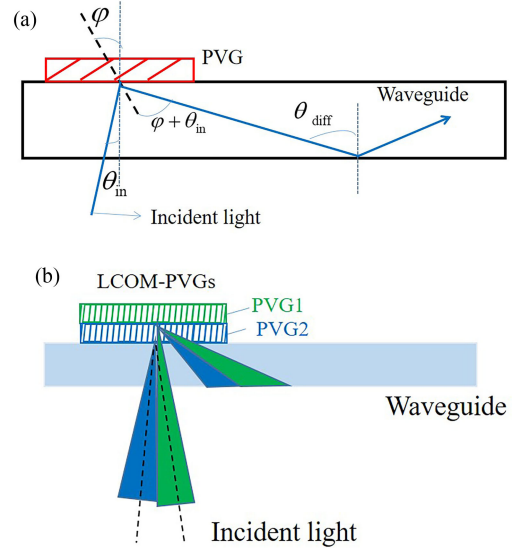

Fig. 2. (a) Propagation mechanism of light beams in waveguide. (b) Schematic diagram of FOV stitching of LCOM-PVGs.

in the y-direction is called the longitudinal period (Λ_y), Λ_b is the Bragg period, and ϕ is the slanted angle of the periodical refractive index planes. According to the geometric relationship, the relationship between Λ_x and Λ_y and Λ_b is:

$$\begin{cases} \Lambda_b = \Lambda_x \sin \phi \\ \Lambda_b = \Lambda_y \cos \phi \\ p = \Lambda_b \end{cases} \quad (1)$$

where p is the pitch of the liquid crystal. At normal incidence, the Bragg period Λ_b of PVG and incident center wavelength λ_b should satisfy the Bragg condition:

$$2n_{eff}\Lambda_b \cos \phi = \lambda_b \quad (2)$$

where n_{eff} is the average refractive index of the anisotropic medium. Supposing the refractive index of the ordinary light of the anisotropic material is n_o and the refractive index of the extraordinary light is n_e, then n_{eff} is represented by:

$$n_{eff} = \sqrt{(n_e^2 + 2n_o^2)/3}. \quad (3)$$

In order to expand the response bandwidth, this paper designs the LCOM-PVGs structure, which stacks gratings with different slanted angles together. In order to avoid ghosting between different PVGs under the same waveguide, which will affect the imaging effect of the waveguide, Λ_x of each layer of PVG is required to be consistent. The structure is shown in Fig. 1(b). To change the tilt angle, we only need to adjust the p. The method of changing the P will be explained in the device fabrication section later.

When the Bragg diffraction condition is satisfied, the propagation mechanism of the light beams in the waveguide is shown in Fig. 2(a) [23]. We can find that the relationship between the diffraction angle θ_{diff} and the incident angle θ_{in} is as follows:

$$\theta_{diff} = 2\phi + \theta_{in} \quad (4)$$

Under non-Bragg conditions, the relationship between the incident angle and the diffraction angle is as follows:

$$\theta_{diff} = \arcsin \left(\frac{\lambda}{\Lambda_x n_{eff}} + \sin \theta_{in} \right) \qquad (5)$$

The propagation angle of light in the waveguide is limited, and the minimum diffraction angle $\theta_{\min}$ is determined by the total internal reflection angle (*TIR*):

$$\theta_{\min} = TIR = \arcsin \left(\frac{1}{n_{glass}} \right) \qquad (6)$$

where n_{glass} is the refractive index of the waveguide medium. At the same time, in order to ensure the continuity of the exit pupil of the waveguide system, the maximum diffraction angle $\theta_{\max}$ in the waveguide is limited by the following equation:

$$\theta_{\max} = \arctan \left(\frac{P_{in}}{2d} \right) \qquad (7)$$

where P_{in} is the exit pupil diameter in the x direction of the collimating system, and d is the waveguide thickness.

The waveguide structure based on LCOM-PVGs is shown in Fig. 2(b). The diffraction angles of PVG1 and PVG2 need to follow:

$$\theta_{\min} \leq \theta_{diff} \leq \theta_{\max} \qquad (8)$$

We perform numerical studies of PVGs and LCOM-PVGs based on the rigorous coupled-wave analysis (RCWA) approach [24]. In the simulation, the horizontal period is set to 431.1 nm. As shown in Fig. 3(a), we simulated the wavelength bandwidth of the single-layer PVG with the center wavelengths of 510 nm and 550 nm and the two single-layer PVG superimposed LCOM-PVGs. (Since the later experimental test uses linearly polarized light, we also set the incident light to linearly polarized light in the simulation, so the efficiency is below 50%.) It can be clearly seen from that the wavelength bandwidth of LCOM-PVGs is approximately 40 nm larger than that of single PVG. And the wavelength bandwidth after stacking covers the bandwidth of the single layer. As shown in Fig. 3(b) and (c), we simulated the diffraction efficiency distribution of PVG and LCOM-PVGs at different incident angles and wavelengths of incident light in the waveguide. Since our AR display uses an OLED image source, we added the normalized OLED spectrum to evaluate the FOV that the holographic waveguide system can achieve. The spectral curve of the OLED image source is shown in Fig. 3(b). The center wavelength of the OLED is 523.52 nm, and the half-wave bandwidth is 29.68 nm. Fig. 3(c) shows that the incident angle range of single PVG with center wavelength of 530 nm (in the waveguide medium) is about 14°. Fig. 3(d) shows that the incident angle range of LCOM-PVGs (PVGs with center wavelength of 510 nm at −5.5° and 550 nm at 6.3°) is about 25°, that is, the horizontal FOV can reach 25°, which is about 11° larger than the single-layer PVG in Fig. 3(c). It is not a double relationship, because we have overlapping parts in the response range when designing. According to the law of refraction, the horizontal FOV in the air can reach 50°, which is in line with the OLED image source with a diagonal field of view of 55° used in the later experiments.
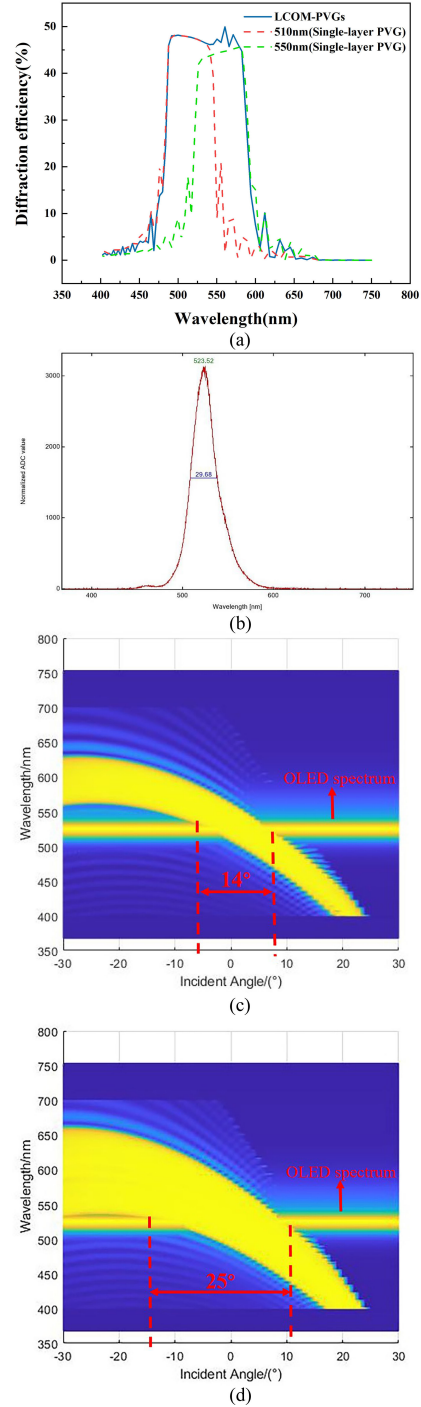

Fig. 3. (a) Simulation of wavelength response curve. (b) OLED image source spectral curve. (c) Simulated angular and spectral responses of single PVG with center wavelength of 530 nm. (d) Simulated angular and spectral responses of LCOM-PVGs.

In order to ensure the optical efficiency of the waveguide display system, the diffraction efficiency of the grating needs to be improved. Due to the polarization characteristics of PVG, for a general light source, if only a single-chiral PVG is used, the light efficiency loss at the in-coupling position will reach more than 50%, and the final image brightness loss at the out-coupling position will reach more than 75%. The polarization
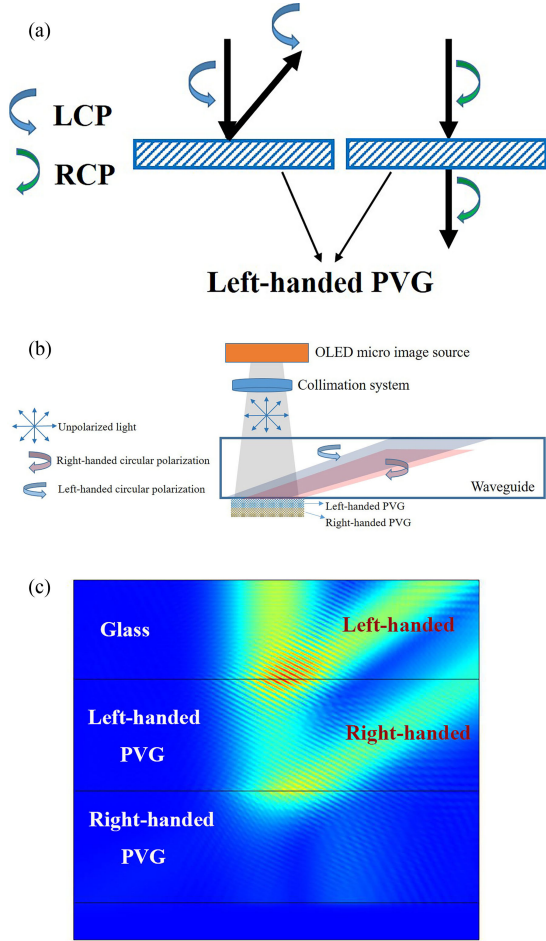
Fig. 4.   (a) Schematic diagram of PVG polarization sensitivity. (b) Schematic diagram of PVG-based polarization multiplexing structure. (c) Simulation of polarization multiplexing based on PVG.
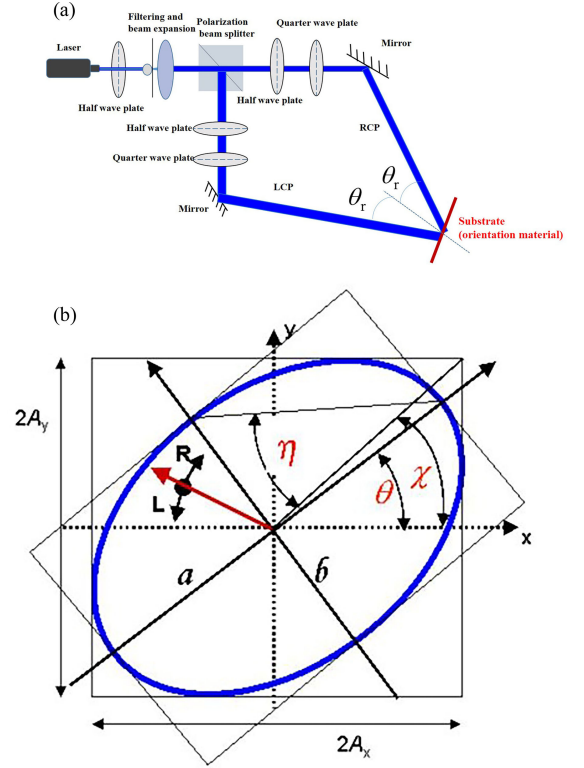

Fig. 5.   (a) Schematic diagram of exposure device. (b) Schematic diagram of the relevant parameters needed to use the polarization measuring instrument.

with polarization multiplexing, that is, the left-handed PVG in Fig. 4(b) uses left-handed LCOM-PVGs, and the right-handed PVG uses right-handed LCOM-PVGs.

III. RESULTS AND DISCUSSION

A. Device Fabrication

The fabrication procedure we adopted is similar to that described by Weng *et al.* [12]. Brilliant Yellow (BY, Sigma) as the alignment layer material was dissolved in dimethylformamide (DMF, Sinopharm Chemical Reagent Co., Ltd.) with a concentration of 0.6wt.%, as the alignment layer solution. The solution is spin-coated (800rpm3s, 3000rpm40s) on the clean glass substrate after ozone cleaning, and then expose. The exposure device is shown in Fig. 5(a), which exposes the substrate (the glass substrate spin-coated with the alignment layer solution) to two beams of left-handed circularly polarized light and right-handed circularly polarized light with orthogonal polarizations to generate a polarization interference pattern. The θ_r and the laser wavelength λ_r determine Λ_x of the PVG:

$$\theta_r = \arcsin\left(\frac{\lambda_r}{2\Lambda_x}\right) \tag{9}$$

Ideally, the interference pattern obtained by using standard circularly polarized light to orientate is the best choice, but if the polarization of the beam is not precisely adjusted, the final beam on the substrate material is likely to be elliptically polarized rather than circularly polarized. Therefore, in order to obtain the final circularly polarized light, it is necessary

characteristics of PVG are shown in Fig. 4(a). When the incident light enters the waveguide vertically, the left-handed PVG will diffract the left-handed circularly polarized light(LCP), the right-handed circularly polarized light(RCP) will pass through, and the right-handed PVG will diffract RCP [11]. When using a polarized image source, we can add a quarter waveplate at the image source to change the incident light into circularly polarized light with the same rotation direction as the PVG, so that the imaging brightness will be greatly improved. When the image source is non-polarized, such as an OLED image source, this paper designs a PVG-based polarization multiplexing structure. This structure is also applicable to polarized image sources. The structure is shown in Fig. 4(b). The in-coupling grating is composed of right-handed PVG and left-handed PVG, which enter the waveguide at the same diffraction angle. Then we used the finite element commercial software COMSOL [11] for simulation to verify the usability of this structure, as shown in Fig. 4(c). In the simulation, the horizontal period is 431.1 nm and the tilt angle is 25.97°. Both LCP and RCP diffract in the same direction with the same diffraction angle.

In order to increase FOV of the waveguide display system while ensuring optical efficiency, we combine the LCOM-PVGs

to use a polarization measuring instrument to help determine the polarization characteristics of the circularly polarized light. During the experiment, the polarization measuring instrument we used is Thorlabs PAX1000. We need to determine the power split ratio (*psr*) of the beam emitted through the quarter wave plate that has not yet reached the sample, and use formulas (10) and (11) to calculate:

$$\tan\eta = \frac{b}{a} = \cos\theta_r \tag{10}$$

$$psr = \frac{1}{2}(1 + \cos 2\theta \cdot \cos 2\eta) \tag{11}$$

The meaning of each parameter in the formula is shown in Fig. 5(b), θ represents the angle between the long axis a of the ellipse and the x-axis, and θ is always 0° in this paper, η is expressed by the ratio of the short axis b to the long axis a, and represents the polarization direction of the beam. $\eta > 0$, $\eta < 0$, and $\eta = 0$ respectively represent right-handed polarization, left-handed polarization, and linear polarization. In this paper, λ_r is 457 nm, θ_r is 32°, *psr* is 0.53 and the exposure dosage is 1 J/cm^2.

After exposure, the sample was placed on a heating table and heated at 80 °C for 2 min. After cooling, the liquid crystal mixture solution (LCMS) was spin-coated with the parameters of 800 rpm for 5 s and 3000 rpm for 40 s. The solvent of LCMS is Toluene (Sinopharm Chemical Reagent Co., Ltd.). The solutes of LCMS include liquid crystal monomer material RM257(Jiangsu Hecheng New Material Co., Ltd.), chiral agent R5011/S5011(Jiangsu Hecheng New Material Co., Ltd.) and photoinitiator IRGACURE 651 (for UV curing, Shanghai yuanye Bio-Technology Co., Ltd). R5011 is used to prepare right-handed PVG, S5011 is used to prepare left-handed PVG. As the main material in the solutes, RM257 mainly determines the thickness of the liquid crystal layer, and the concentration generally does not exceed 20%. P is determined by the *HTP* of R5011/S5011 and the concentration c[25], [26]:

$$p = (HTP \cdot c)^{-1} \tag{12}$$

The desired p for each PVG were generated after the spin-coating of prepared chiral-dopant LCMS. Therefore, we only need to change c to prepare LCOM-PVGs. Then, the sample was heated at 80 °C for 3 minute. This heating step is an indispensable step, which affects the arrangement of the liquid crystal molecules, as shown in Fig. 6, the arrangement of the liquid crystal molecules after heated (A) and unheated (B) was photographed with a polarizing microscope (Nikon, LV100N). The bright stripes in Fig. 6(a) are parts where the liquid crystal molecules are not completely aligned. Meanwhile, we can find in the Fig. 6 that the horizontal period (430 nm) prepared is basically equivalent to the designed value of 431.1 nm. Finally, the coated substrate was cured with 365 nm UV light in a nitrogen environment.

Fig. 7 shows the polarization multiplexed waveguide structure based on LCOM-PVGs. In the actual preparation, we prepared the right-handed LCOM-PVGs and left-handed LCOM-PVGs on different waveguides, then sprayed spacers with a thickness of 5 μm on one of the waveguides, and then packaged them with
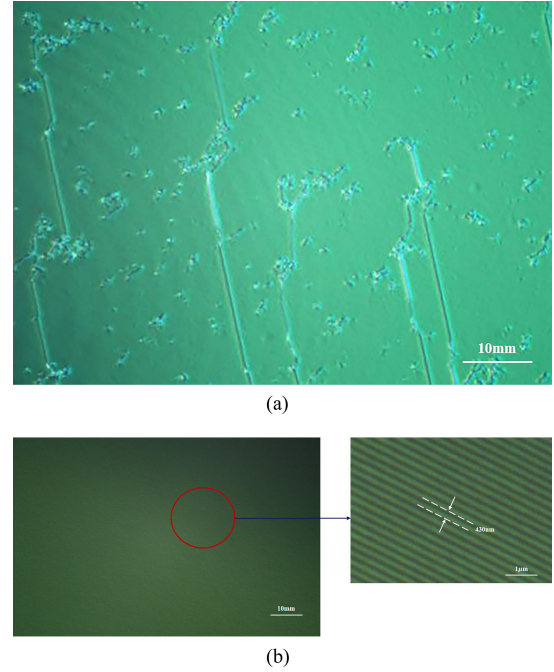

Fig. 6. Polarizing microscopy images of the liquid crystal molecules after (a) heated (b) unheated.
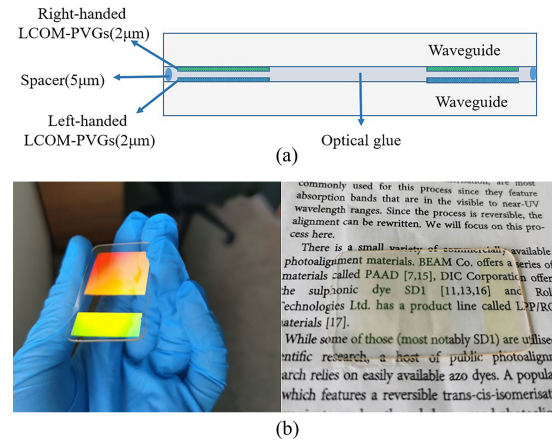

Fig. 7. (a) Schematic diagram of the polarization multiplexed waveguide structure based on LCOM-PVGs. (b) The appearances of the waveguide with LCOM-PVGs in an indoor white luminance environment (left). Photo taken through the waveguide that shows good transparency for the fabricated LCOM-PVGs (right).

curable optical glue matching the refractive index of the grating, as shown in Fig. 7(a). Fig. 7(b) represents the appearances of the waveguide with LCOM-PVGs. We can observe a bright grating diffraction in an indoor white luminance environment with different view angles and good transparency of the waveguide. According to (8), the refractive index of the waveguide medium determines the lower limit of the diffraction angle. The larger the refractive index, the larger the range of the propagation angle, and the larger the field of view that can be supported. The upper limit of the propagation angle is determined by P_{in} and the waveguide thickness d. Since the diagonal field of view in the air supported by the AR machine used in the experiment is 55°, in order to ensure that the propagation angle range is large
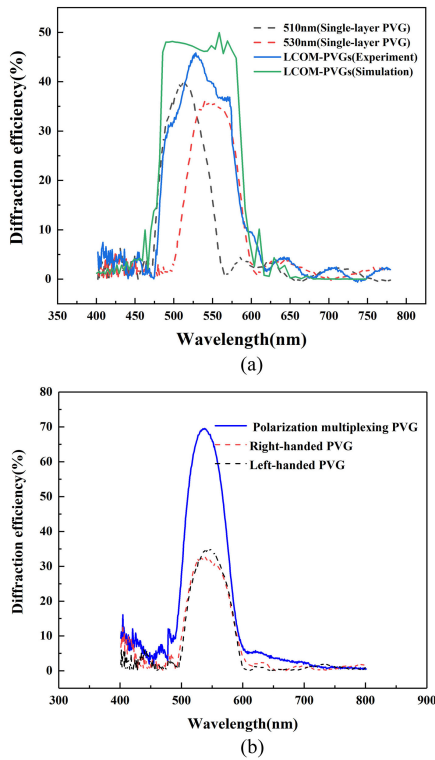
(a)

(b)

Fig. 8. Experimental diffraction efficiency spectra for (a) the LCOM-PVGs. (b) the polarization multiplexing structure with normal incidence.

(a)

(b)

(c)

Fig. 9. (a) Physical image of holographic waveguide display module. (b) Input image. (c) Actual display effect picture in a bright indoor environment based on PVG and LCOM-PVGs.

enough, optical glass with a refractive index of 1.8 is selected as the substrate, P_{in} is 20mm, and d is 0.7 mm, so the maximum diffraction angle is 85.99°.
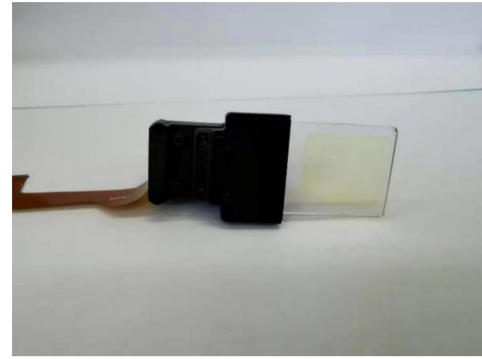
B. Response Bandwidth Test

The wavelength bandwidth of LCOM-PVGs was measured with a fiber optic spectrometer(Shanghai Ideaoptics Corporation, R1), as shown in Fig. 8(a). Since the incident light is linearly polarized during the measurement, the efficiency is less than 50%. The experimental results are basically consistent with the simulation results. The wavelength bandwidth of single-layer PVG with center wavelengths of 510 nm and 550 nm is around 60 nm, and the wavelength bandwidth after stacking can reach 100 nm. In addition, the diffraction efficiency is lower than the simulation result, the possible reason is that some disturbed alignment would decrease the diffraction efficiency [15].

We also measured the diffraction efficiency using the polarization multiplexing structure, as shown in Fig. 8(b). It can be seen that compared with a single left-handed LCOM-PVGs or right-handed LCOM-PVGs, the efficiency of the polarization multiplexing structure has increased by nearly two times, indicating that the use of this structure can indeed enhance the optical efficiency of the waveguide structure.

C. AR Display Application

We measured the light luminance from a D65 light source before and passing through the out-couplers area and obtained a 72% transmittance. The good transparency is conducive to the

ambient light transmittance of the waveguide display system and meets the requirements of the combination of virtual and real in AR applications. In order to verify the performance of the grating coupler we fabrication, the grating coupler was placed on the AR display module as shown in Fig. 9(a), which contains a high-brightness silicon-based OLED microdisplay, a collimating optical lens group and a waveguide sheet. The AR display module was designed to provide a max diagonal FOV of 55°. Fig. 9(b) shows the input image of the image source. Fig. 9(c) compares the display effect of the waveguide based on LCOM-PVGs and PVG. The camera employed to capture the output image was placed in front of the out-coupler with the designed eye-relief of 18 mm. We can see that the complete output within the range of 55° diagonal FOV cannot be achieved using a single PVG. However, the image was fully and clearly observed without significant color shift and distortion using

LCOM-PVGs. Furthermore, we use AR/VR lens with ProMetric I8 camera (Radiant Vision Systems) to test the actual FOV of the prototype. The test results show that the horizontal FOV is 43.6°, the longitudinal FOV is 34°, and the diagonal FOV is 55.3°, which is basically consistent with the design values.

From Fig. 9(c) it can be found that the imaging brightness is not uniform. The reason for the phenomenon is that the first exit pupil is higher due to the high efficiency of the out-coupling grating, and the rear exit pupil is lower. In the following work, this problem can be improved through efficiency distribution control.

In this paper, we also use the nine-point method [27] to test the brightness L_d of the silicon-based OLED microdisplay and the virtual image brightness L_w of the holographic waveguide display module. First, the brightness of nine points in the display screen of OLED microdisplay is tested with a spot luminance meter CS-200, and then the average brightness of the OLED microdisplay is calculated to be 7648 cd/m^2, and then measure the brightness of the virtual image with the same method. The brightness of the virtual image without the polarization multiplexing structure is 596 cd/m^2, while the polarization multiplexing structure is 1100 cd/m^2. The optical imaging efficiency is L_w/L_d. According to calculation, the imaging efficiency of the module without the polarization multiplexing structure is 7.8%, and the imaging efficiency with the polarization multiplexing structure is 14.3%. Similarly, we can build a colorful holographic waveguide display by using polarization multiplexing structure based on LCOM-PVGs. Compared with the previous work [12], [16], both the brightness and the field of view have been significantly improved.

IV. Conclusion

In this paper, the structure of LCOM-PVGs is proposed to increase the bandwidth of PVG, and the polarization multiplexing structure based on PVG is proposed to enhance the optical efficiency, and the feasibility is verified through experimental preparation. Next, we prepare a polarization multiplexing structure waveguide based on LCOM-PVGs, the wavelength response bandwidth can be increased by 40 nm, and the efficiency can be increased by nearly twice. We also demonstrated the display performance on the AR display. The results show that images with a diagonal FOV of about 55° can be clearly displayed, and the measured total optical efficiency is as high as 14.3% with a transparency of 72% for ambient light. This work verifies the effectiveness of laminated gratings in improving the response bandwidth of PVG, and provides a practical technical route for holographic waveguides to achieve large field of view and high brightness.

References

[1] K. Yin, Z. He, J. Xiong, J. Zou, K. Li, and S.-T. Wu, "Virtual reality and augmented reality displays: Advances and future perspectives," *J. Phys.: Photon.*, vol. 3, no. 2, pp. 022010–022023, 2021.

[2] B. C. Kress, "Optical waveguide combiners for AR headsets: Features and limitation," in *Proc. Digit. Opt. Technol.*, vol. 11062, no. 10620J, 2019, pp. 1–26.

[3] Z. Zhuang, Q. Cheng, P. Surman, Y. Zheng, and X. W. Sun, "A compact and lightweight off-axis lightguide prism in near to eye display," *Opt. Commun.*, vol. 393, pp. 143–151, 2017.

[4] D. Cheng, Y. Wang, C. Xu, W. Song, and G. Jin, "Design of an ultra-thin near-eye display with geometrical waveguide and freeform optics," *Opt. Exp.*, vol. 22, no. 17, pp. 20705–20719, 2014.

[5] A. Maimone, A. Georgiou, and J. S. Kollin, "Holographic near-eye displays for virtual and augmented reality," *ACM Trans. Graph.*, vol. 36, no. 4, pp. 1–16, 2017.

[6] J. Xiong, Y. Li, K. Li, and S.-T. Wu, "Aberration-free pupil steerable maxwellian display for augmented reality with cholesteric liquid crystal holographic lenses," *Opt. Lett.*, vol. 46, no. 7, pp. 1760–1763, 2021.

[7] A. Cameron, "Optical waveguide technology and its application in head-mounted displays," in *Proc. Head- Helmet-Mounted Displays XVII; Display Technol. Appl. for Defense, Secur., Avionics VI*, vol. 8383, no. 83830E, 2012, Art. no. 12.

[8] H. Liu, Z. Zheng, H. Li, and X. Liu, "Design of semi-permeable membrane array flat panel display," *Optoelectron. Eng.*, vol. 39, no. 5, pp. 145–150, 2012.

[9] G. Bianco *et al.*, "Volume holographic gratings: Fabrication and characterization," in *Proc. Spie Int. Soc. for Opt. Eng.*, 2015, pp. 950807.1–950807.7.

[10] S. Moujdi, A. Rahmouni, T. Mahfoud, D. V. Nesterenko, M. Halim, and Z. Sekkat, "Surface relief gratings in azo-polymers revisited," *J. Appl. Phys.*, vol. 124, no. 21, pp. 213103.1–221303.9, 2018.

[11] Y. Weng, D. Xu, Y. Zhang, X. Li, and S.-T. Wu, "Polarization volume grating with high efficiency and large diffraction angle," *Opt. Exp.*, vol. 24, no. 16, pp. 17746–17759, 2016.

[12] Y. Weng *et al.*, "Liquid-crystal-based polarization volume grating applied for full-color waveguide displays," *Opt. Lett.*, vol. 43, no. 23, pp. 5773–5776, 2018.

[13] K. Yin, H.-Y. Lin, and S.-T. Wu, "Stretchable, flexible, and adherable polarization volume grating film for waveguide-based augmented reality displays," *J. Soc. for Inf. Display*, vol. 27, no. 4, pp. 232–237, 2019.

[14] Z. He, Y. H. Lee, K. Yin, and S. T. Wu, "Recent advances in liquid-crystal polarization volume gratings," in *Proc. Liquid Crystals XXIII*, vol. 11092, no. 1109204, 2019, pp. 1–10.

[15] K. Yin, H.-Y. Lin, and S.-T. Wu, "Chirped polarization volume grating for wide FOV and high efficiency waveguide-based AR displays," *J. Soc. Inf. Display*, vol. 28, no. 4, pp. 368–374, 2020.

[16] J. Cui and Y. Zhang, "Exit pupil expansion based on polarization volume grating," *Crystals*, vol. 11, no. 4, 2021, Art. no. 333.

[17] T. Zhan *et al.*, "Pancharatnam-Berry optical elements for head-up and near-eye displays invited," *J. Opt. Soc. Amer. B-Opt. Phys.*, vol. 36, no. 5, pp. D52–D65, 2019.

[18] Y. Sulai, M. Geng, and S. Luanava, "Field of view: Not just a number," presented at the Proc. Digital Optics for Immersive Displays (DOID18), 2018.

[19] K. Yin, H. Y. Lin, and S. T. Wu, "Chirped polarization volume grating with ultra-wide angular bandwidth and high efficiency for see-through near-eye displays," *Opt. Exp.*, vol. 27, no. 24, pp. 35895–35902, 2019.

[20] X. Xiang, J. Kim, and M. J. Escuti, "Bragg polarization gratings for wide angular bandwidth and high efficiency at steep deflection angles," *Sci. Rep.*, vol. 8, no. 1, 2018, Art. no. 7202.

[21] J. Xiong, R. Chen, and S.-T. Wu, "Device simulation of liquid crystal polarization gratings," *Opt. Exp.*, vol. 27, no. 13, pp. 18102–18112, 2019.

[22] Y. H. Lee, Z. He, and S. T. Wu, "Optical properties of reflective liquid crystal polarization volume gratings," *J. Opt. Soc. Amer. B*, vol. 36, no. 5, pp. D9–D12, 2019.

[23] Z. Shen, Y. Zhang, Y. Weng, and X. Li , "P-103: Optimization of field of view and color uniformity in a holographic waveguide display," in *Proc. Sid Symp. Dig. Tech. Papers*, vol. 48, no. 1, 2017, pp. 1634–1637.

[24] J. Xiong and S.-T. Wu, "Rigorous coupled-wave analysis of liquid crystal polarization gratings," *Opt. Lett.*, vol. 28, no. 24, pp. 35960–35971, 2020.

[25] D. J. Earl and M. R. Wilson, "Predictions of molecular chirality and helical twisting powers: A theoretical study," *J. Chem. Phys.*, vol. 119, no. 19, pp. 10280–10288, 2003.

[26] J. Lub, D. J. Broer, R. T. Wegh, E. Peeters, and B. M. I. van der Zande, "Formation of optical films by photo-polymerisation of liquid crystalline acrylates and application of these films in liquid crystal display technology," *Mol. Crystals Liquid Crystals*, vol. 429, no. 1, pp. 77–99, 2006.

[27] *People's Republic of China Electronics Industry Standard SJ/T 11281-2017 Light-emitting diode (LED) Display Test Method*, Beijing, China: Ministry of Information Industry of the People's Republic of China, 2017.